Observation of the geometric spin Hall effect of light

Jan Korger,[1,2] Andrea Aiello,[1,2,*] Vanessa Chille,[1,2] Peter Banzer,[1,2] Christoffer Wittmann,[1,2] Norbert Lindlein,[2] Christoph Marquardt,[1,2] and Gerd Leuchs[1,2]

[1] *Max Planck Institute for the Science of Light, Erlangen, Germany*
[2] *Institute for Optics, Information and Photonics, University Erlangen-Nuremberg, Germany*

(Dated: March 27, 2013)

The spin Hall effect of light (SHEL) is the photonic analogue of spin Hall effects occurring for charge carriers in solid-state systems.[1–3] A prime example of this intriguing phenomenon occurs when a light beam refracts at an air-glass interface. It amounts to a polarization-dependent displacement perpendicular to the plane of incidence. At optical wavelengths, this shift is about a few tens of nanometres. Recently, it was predicted that a light beam projected onto an oblique plane can undergo a significantly larger displacement:[4,5] This effect, named geometric SHEL, is a consequence of spin-orbit coupling and is largely independent from the physical implementation of the projection. Here, we experimentally demonstrate this novel phenomenon by observing an optical beam transmitted across an oblique polarizer. The spatial intensity distribution of the transmitted beam depends on the incident state of polarization and its centroid undergoes a positional displacement exceeding one wavelength. This novel type of spin-orbit coupling is unavoidable for light fields carrying angular momentum and practically relevant for any precision measurement using polarized beams.

Already in 1943, Goos and Hänchen observed that the position of a light beam totally reflected from a glass-air interface differs from metallic reflection.[6] This is the most well-known example of a longitudinal beam shift occurring at the interface between two optical media. In honour of their seminal work, any such deviation from geometrical optics occurring in the plane of incidence, is referred to as a Goos-Hänchen shift. Conversely, a similar shift occurring in a direction perpendicular to the plane of incidence is known as Imbert-Fedorov shift.[7,8] These phenomena generally depend both on properties of the incident light beam and the physical interaction occurring at an interface.[9] Goos-Hänchen and Imbert-Fedorov shifts have been observed at dielectric,[10] semiconductor[11] and metal[12] interfaces.

The Imbert-Fedorov shift[7,8,13] is an example of the spin-Hall effect of light (SHEL) arising at a planar interface between two dielectric media. SHEL is a consequence of the spin-orbit interaction (SOI) of light, namely the coupling between the spin and orbital angular momentum in an optical field.[1,2,4,14–22] All electromagnetic SOI phenomena in vacuum and in locally isotropic media can be interpreted in terms of the geometric Berry phase and angular momentum dynamics.[23] For a freely propagating paraxial beam of light, SOI effects vanish unless a relevant breaking of symmetry occurs. A typical example of such a symmetry break is the interaction of the beam with an oblique surface, whose normal lies under an angle θ with respect to the beam axis (see Figure 1).

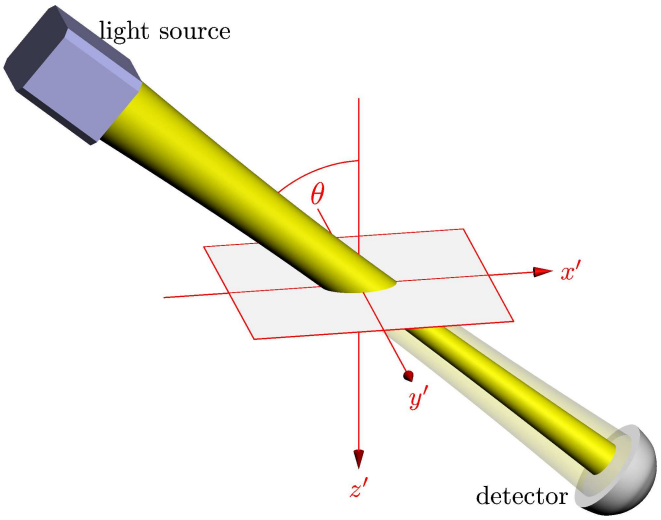

Figure 1. **Spin Hall effects of light occur when a light beam propagates across an oblique interface.** The presence of a surface not perpendicular to the direction of beam propagation breaks the symmetry of the incident beam. This can give rise to spin-orbit coupling, which manifests itself as a spin-dependent displacement of the transmitted beam. In this work, we specifically study light beams impinging under an angle θ onto a polarizing interface. The reference frame $\{\boldsymbol{x}', \boldsymbol{y}', \boldsymbol{z}'\}$ is aligned with the polarizer surface.

Although the resulting phenomena essentially depend on the type of the interaction with the surface,[24] there are some common characteristics that reveal universality in SOI of light due to the geometry and the dynamical angular momentum aspects of the problem. Amongst the various observable effects resulting from the beam-surface interaction, the so-called *geometric Hall effect of light* is virtually independent from the properties of the surface[4,5,25,26] and, therefore, represents the ideal candidate for studying above-mentioned universal features. It amounts to a shift of the centroid of the intensity distribution represented by Poynting-vector flow of the beam across the oblique surface of a tilted detector. Direct observation of this effect as originally proposed depends critically on the detector's response to the light field.

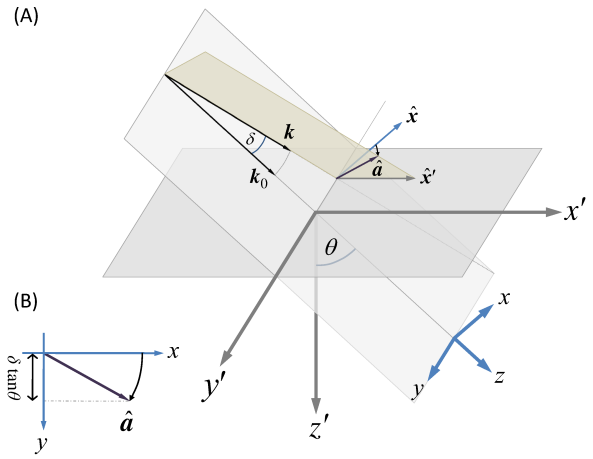

Figure 2. **The geometric SHEL at a polarizing interface.** (A) The horizontal dark grey plane represents the polarizing interface with the Cartesian reference frame $\{\boldsymbol{x}', \boldsymbol{y}' \equiv \boldsymbol{y}, \boldsymbol{z}'\}$ attached to it. The axis $\hat{\boldsymbol{x}}'$ is taken parallel to the absorbing axis of the polarizing interface. $\theta \in [0, \pi/2)$ denotes the angle of incidence. The central wave vector $\boldsymbol{k}_0$ of the incident beam defines the direction of the axis $\hat{\boldsymbol{z}}$ of the frame $\{\boldsymbol{x}, \boldsymbol{y}, \boldsymbol{z}\}$ attached to the beam. It is instructive to study a wave vector $\boldsymbol{k}$ in the z-y-plane, rotated by an angle $\delta \ll 1$ with respect to $\boldsymbol{k}_0$. (B) The unit vector $\hat{\boldsymbol{a}} \perp \boldsymbol{k}$, representing the direction of the absorbed component of the incident field, lies in the common plane of $\boldsymbol{k}$ and $\hat{\boldsymbol{x}}'$ (coloured light brown in the figure) and can be obtained, in the first-order approximation, from the rotation by the angle $\delta \tan\theta$ around $\boldsymbol{k}$, of the unit vector $\hat{\boldsymbol{x}}$.

However, the question whether the response function of a real detector is indeed proportional to the Poynting vector density is subject to a long-standing debate.[27,28]

In this work, we implement an alternative scheme,[5] in which the occurrence of the beam shift is independent of the detector response. To this end, we send a circularly polarized beam of light across a tilted polarizing interface to demonstrate a novel kind of geometric Hall effect, in which the centroid of the resulting linearly polarized transmitted beam undergoes a spin-induced transverse shift up to several wavelengths. This approach is different from the early proposal[4] in that it is observable with standard optical detectors. Furthermore, it is different from the SHEL occurring in a beam passing through an air-glass interface[2] since this geometric SHEL is practically independent of Snell's law and the Fresnel formulas for the interface.

As for conventional SHEL, the physical origin of this geometric version resides in the SOI of light. In fact, we can describe this effect in terms of the geometric phase generated by the spin-orbit interaction as follows: When the beam passes through the polarizing interface, the plane wave components with different wave vectors acquire different geometric phases determined by distinct local projections yielding to effective "rotations" of the polarization vector around the wave vector. The interference of these modified plane waves produces a redistribution of the intensity spatial profile of the beam resulting in a spin-dependent transverse shift of the intensity centroid.

This effect can be better understood with the help of Figure 2 that illustrates the geometry of the problem. The incident monochromatic beam can be thought of as made of many plane wave components with wave vectors $\boldsymbol{k}$ spreading around the central one $\boldsymbol{k}_0 = k\hat{\boldsymbol{z}}$, which represents the main direction of propagation of the beam, where $|\boldsymbol{k}_0| = k = |\boldsymbol{k}|$. For a well-collimated beam, the angle between an arbitrary wave vector $\boldsymbol{k}$ and the central one $\boldsymbol{k}_0$ is, by definition, small: $\delta \ll 1$. In the first-order approximation with respect to δ, we consider $\boldsymbol{k} = k(\hat{\boldsymbol{z}}\cos\delta - \hat{\boldsymbol{y}}\sin\delta) \cong k(\hat{\boldsymbol{z}} + \kappa_y\,\hat{\boldsymbol{y}})$, where $\kappa_y \equiv k_y/k = -\sin\delta \cong -\delta$. The either left- ($\sigma = +1$) or right-handed ($\sigma = -1$) circular polarization of the incident beam is determined by the unit vector $\hat{\boldsymbol{u}}_\sigma = (\hat{\boldsymbol{x}} + i\sigma\hat{\boldsymbol{y}})/\sqrt{2}$ globally defined with respect to the axis $\hat{\boldsymbol{z}}$ of the beam frame $\{\hat{\boldsymbol{x}}, \hat{\boldsymbol{y}}, \hat{\boldsymbol{z}}\}$. However, from Maxwell's equations it follows that the divergence of the electric field of a light wave in vacuum is zero. This requires that the polarization $\hat{\boldsymbol{e}}_\sigma(\boldsymbol{k})$ of each plane wave component of wave vector $\boldsymbol{k}$ must necessarily be transverse, namely $\boldsymbol{k}\cdot\hat{\boldsymbol{e}}_\sigma(\boldsymbol{k}) = 0$. This requirement is clearly not satisfied by $\hat{\boldsymbol{u}}_\sigma$ for which one has $\boldsymbol{k}\cdot\hat{\boldsymbol{u}}_\sigma/k \cong i\sigma\kappa_y/\sqrt{2} \neq 0$. Anyhow, the transverse nature of the light field can be easily restored by subtracting from $\hat{\boldsymbol{u}}_\sigma$ its longitudinal component: $\hat{\boldsymbol{u}}_\sigma \to \hat{\boldsymbol{e}}_\sigma(\boldsymbol{k}) \propto \hat{\boldsymbol{u}}_\sigma - \boldsymbol{k}\,(\boldsymbol{k}\cdot\hat{\boldsymbol{u}}_\sigma)\,/k^2 \cong \hat{\boldsymbol{u}}_\sigma - (i\sigma\,\kappa_y/\sqrt{2})\hat{\boldsymbol{z}}$. Now that we have properly modeled the polarization of the incident field, let us see how it changes when the beam crosses the polarizing interface.

A linear polarizer is an optical device that absorbs radiation polarized parallel to a given direction, say $\hat{\boldsymbol{x}}'$, and transmits radiation polarized perpendicular to that direction. The electric field of each plane wave component of the beam sent through the polarizing interface, changes according to the projection rule $\hat{\boldsymbol{e}}_\sigma(\boldsymbol{k}) \to \hat{\boldsymbol{e}}_\sigma(\boldsymbol{k}) - \hat{\boldsymbol{a}}(\hat{\boldsymbol{a}}\cdot\hat{\boldsymbol{e}}_\sigma(\boldsymbol{k})) = \hat{\boldsymbol{t}}(\hat{\boldsymbol{t}}\cdot\hat{\boldsymbol{e}}_\sigma(\boldsymbol{k}))$, where $\boldsymbol{a} = \hat{\boldsymbol{x}}' - \boldsymbol{k}(\boldsymbol{k}\cdot\hat{\boldsymbol{x}}')/k^2$ is the effective absorbing axis with $\hat{\boldsymbol{a}} = \boldsymbol{a}/|\boldsymbol{a}| \cong \hat{\boldsymbol{x}} - \hat{\boldsymbol{y}}\,\kappa_y\tan\theta$, and $\hat{\boldsymbol{t}} = \hat{\boldsymbol{a}}\times\boldsymbol{k}/k$ is the effective transmitting axis. The key term to calculate is the transmitted amplitude $\hat{\boldsymbol{t}}\cdot\hat{\boldsymbol{e}}_\sigma(\boldsymbol{k}) \propto (1 - i\sigma\kappa_y\tan\theta)/\sqrt{2} \cong \exp(-i\sigma\kappa_y\tan\theta)/\sqrt{2}$, where an irrelevant κ_y-independent overall phase factor has been omitted.

Therefore, as a result of the transmission, the amplitude of each plane wave component is reduced by a factor $1/\sqrt{2}$ and multiplied by the *geometric phase* term $\exp(-i\sigma\kappa_y\tan\theta)$. Here, the "$\tan\theta$" behavior of the phase, characteristic of the geometric SHEL,[4] is in striking contrast to the typical "$\cot\theta$" angular dependence of the conventional SHEL as, e. g., the Imbert-Fedorov shift.[29] However, the spin-orbit interaction term $\sigma\kappa_y$, expressing the coupling between the spin σ and the transverse momentum κ_y of the beam, is characteristic of both phenomena, thus revealing their common physical origin.

The appearance of the geometric phase term $\exp(-i\sigma\kappa_y \tan\theta)$ leads to a beam shift along the axis $\hat{\boldsymbol{y}}$. This can be seen by writing the incident circularly polarized paraxial beam as $\boldsymbol{\Psi}^{\text{in}}(y) = \hat{\boldsymbol{u}}_\sigma \psi_\sigma^{\text{in}}(y)$, where only the dependence on the relevant transverse coordinate y has been explicitly displayed, and $\psi_\sigma^{\text{in}}(y) = \int \widetilde{\psi}_\sigma^{\text{in}}(\kappa_y) \exp(ik\kappa_y y)\mathrm{d}\kappa_y$. After transmission across the polarizing interface, the Fourier transform $\widetilde{\psi}_\sigma^{\text{in}}(\kappa_y)$ of $\psi_\sigma^{\text{in}}(y)$ changes to $\widetilde{\psi}_\sigma^{\text{in}}(\kappa_y)\exp(-i\sigma\kappa_y\tan\theta)/\sqrt{2}$ and the output field can be written as $\psi_\sigma^{\text{out}}(y) = (1/\sqrt{2})\int \widetilde{\psi}_\sigma^{\text{in}}(\kappa_y)$ $\exp[ik\kappa_y(y - \sigma\tan\theta/k)]\mathrm{d}\kappa_y = (1/\sqrt{2})\psi_\sigma^{\text{in}}(y - \sigma\tan\theta/k)$. This last expression clearly shows that the scalar amplitude of the output field is equal, apart from the $(1/\sqrt{2})$ factor, to the amplitude of the input field transversally shifted by $\sigma\tan\theta/k$. In summary, for circular input polarization the position of the centroid of the transmitted beam is given by

$$\langle y \rangle = \frac{\int y\,|\psi_\sigma^{\text{out}}(y)|^2 \mathrm{d}y}{\int |\psi_\sigma^{\text{out}}(y)|^2 \mathrm{d}y} = \frac{\sigma}{k}\tan\theta, \tag{1}$$

where $k = \frac{2\pi}{\lambda}$. (Please refer to the Supplementary Information for a detailed calculation of this result.)

In the experiment, we use a Corning Polarcor polarizer, made of two layers of elongated and oriented silver nanoparticles embedded in a 25 mm × 25 mm × 0.5 mm glass substrate. Interaction with these particles effectively polarizes the transmitted beam. In order to avoid parasitic effects from the glass surfaces ($n_G = 1.517$), we have submerged the polarizer in a tank with index matching liquid (Cargille laser liquid 5610, $n_L = 1.521$). Without this liquid, the effective tilting angle inside the glass polarizer would be limited by Snell's law to $\arcsin(1/n_G) \approx 41°$.

The polarizer used in this work can be described by its absorbing axis – the orientation of the nano-particles – and two empirical parameters describing transmittance and extinction ratio as a function of the tilting angle θ. Please refer to the SI for an experimental characterization of the device and a phenomenological model.

In our setup (Figure 3), a fundamental Gaussian light beam ($\lambda = 795$ nm) is prepared with the state of polarization alternating between left- ($\sigma = +1$) and right-hand ($\sigma = -1$) circular. By simultaneously observing the position of the light beam transmitted across a polarizing interface and the incident state of polarization, we can determine the helicity-dependent beam shift $\Delta = 2\langle y \rangle$.

It is possible to observe different beam shifts in two configurations. First, we measure the displacement $\Delta_T = 2\langle y \rangle_{|\boldsymbol{E}_T|^2}$ of the total transmitted energy density distribution $|\boldsymbol{E}_T|^2$ when switching the incident state of polarization from $\sigma = +1$ to $\sigma = -1$ (Figure 4(a)). Then, we employ an additional polarization analyzer in front of the detector and observe the shift $\Delta_y = 2\langle y \rangle_{|E_y|^2}$ of the energy density $|E_y|^2 = |\boldsymbol{E}_T \cdot \hat{\boldsymbol{y}}|^2$ of the vertically polarized field component solely (Figure 4(b)). These variants of the experiment coincide for polarizers with perfect extinction ratios but can differ significantly for real-world polarizers with minor deficiencies.

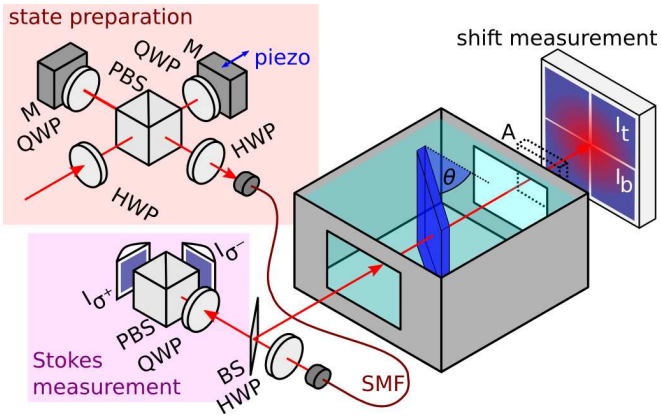

Figure 3. **Experimental Setup: Simultaneous measurement of the incident state of polarization and the position of a light beam transmitted across a tilted polarizer.** State preparation: The relative phase between horizontally and vertically polarized components is modulated using a polarizing beam splitter (PBS), a piezo mirror (M), quarter and half wave plates (QWP, HWP). The beam is spatially filtered using a single-mode fibre (SMF). Stokes measurement: The transmitted port of a beam splitter (BS) is used to monitor the state of polarization. We acquire the Stokes parameters S_3, which distinguishes left- and right-hand circular polarization. Shift measurement: The beam is propagated across our sample, a tank containing a glass polarizer and an index-matching liquid, and its position is observed using a quadrant detector. An optional PBS (A) can be employed as an analyzer in front of the detector. The photo currents $I_{\sigma+}$, $I_{\sigma-}$, I_t, and I_b are amplified and digitally sampled.

The beam shift observed in the latter case increases proportionally to the tangent of the tilting angle, exceeding one wavelength. This characteristic "$\tan\theta$"-dependence, especially close to grazing incidence $\theta \to 90°$, is unique to the geometric spin Hall effect of light.

To the best of our knowledge, this is the first direct measurement of this intriguing phenomenon. The geometric spin Hall effect of light should not be confused with the conventional SHEL or Imbert-Fedorov shift. The latter occurs at a physical interface and, while such interfaces are present in our experimental setup, they can only give rise to beam shifts significantly smaller than the observed effect. In Figure 5, we compare our results to the Imbert-Fedorov shift, which could occur at the polarizer substrate, for a set of realistic parameters.[18,29] This illustrates that the beam shifts measured in this work constitute a novel spin Hall effect of Light, virtually independent from surface effects.

In conclusion, we have presented a novel beam shift occurring at an oblique polarizing interface. To test this geometric spin Hall effect of light experimentally, a circularly polarized laser beam was propagated across a suitable polarizer. We have demonstrated that the centre

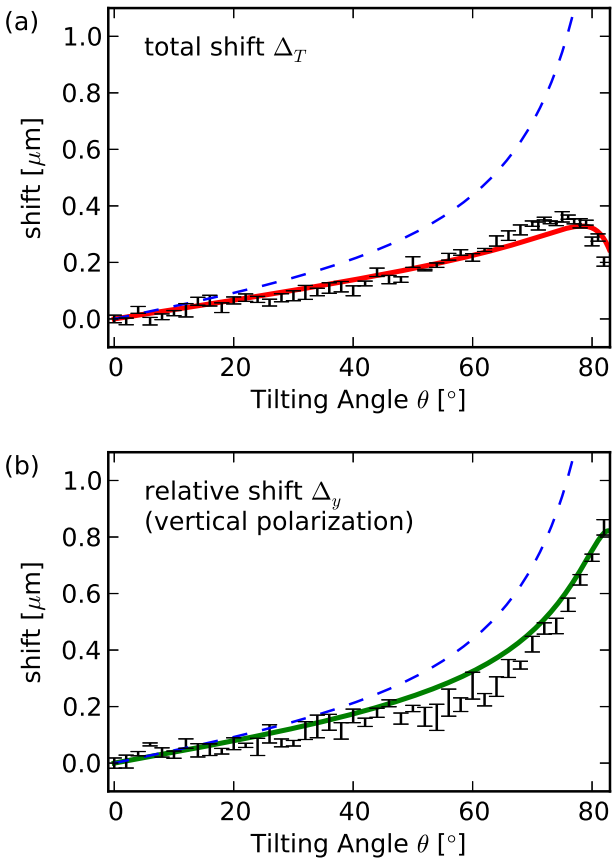

Figure 4. **Polarization-dependent beam shifts occurring at a tilted polarizer.** Measurement data and two theoretical curves are shown. The dashed blue line shows the theory for an ideal polarizer, while the solid lines were calculated from a realistic polarizer model as derived in the SI. Error bars indicate the statistical standard error of the mean. **(a)** Overall displacement Δ_T of the intensity barycentre after transmission across the polarizer. **(b)** Displacement Δ_y of the vertically polarized intensity component solely.

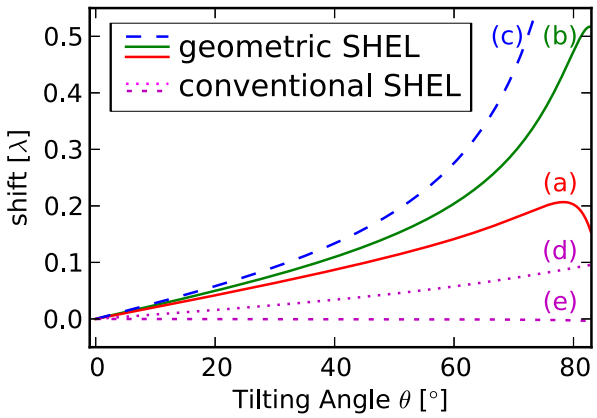

Figure 5. **Conventional spin Hall effect of light compared to the geometric SHEL.** A light beam transmitted across an interface between two media can undergo a transverse displacement known as the Imbert-Fedorov effect or conventional SHEL. Here, we plot this displacement for a left-hand circularly polarized beam ($\sigma = +1$) for two different cases and compare this with the geometric SHEL studied in this work. **(a)** and **(b)** Geometric SHEL $\frac{1}{2}\Delta_T$ and $\frac{1}{2}\Delta_y$ for the two configurations studied experimentally (Figure 4). **(c)** Geometric SHEL as predicted for an ideal polarizing interface. **(d)** Conventional SHEL occurring at an air-glass interface ($n_1 = 1$, $n_2 = 1.5$). **(e)** Conventional SHEL expected for the entrance face of our submerged polarizer ($n_1 = n_L = 1.521$, $n_2 = n_G = 1.517$).

of mass of the transmitted light field is displaced with respect to position of the incident beam as predicted by the theory. While a Gaussian light beam itself is invariant with respect to rotation around its axis of propagation, the geometry induced by the tilted polarizer, breaks this symmetry. This amounts to a spin-to-orbit coupling characteristic for spin Hall effects of light.

METHODS

The state preparation setup (Figure 3) was aligned such that the intensities of vertically and horizontally polarized components were constant and equal. The relative phase between these components was modulated with a frequency of $f_{\mathrm{mod}} = 29\,\mathrm{Hz}$. We have used a single mode fibre to clean the spatial profile and two half-wave plates to compensate for the polarization change due to the fibre. Those wave plates before and after the fibre were aligned such that the combined operation of wave plates and fibre is reduced to a phase shift. We collimated the light beam using an aspheric lens (New Focus 5724-H-B) and aligned its focus such that the beam waist is at the position of the detector.

In order to simultaneously measure the beam position $\langle y \rangle$ and the incident state of polarization, we employed a dielectric mirror (Layertec 103210) as a non-polarizing beam splitter. At an angle of incidence of 3°, transmittance, reflectivity, and phase shift coincide for s and p polarization within experimental accuracy. We have verified this important characteristic of our beam splitter by simultaneously measuring the states of polarization of the transmitted and reflected beams. To this end, we can replace the sample in the transmitted beam path with another Stokes measurement setup.

The beam reflected from the beam splitter was propagated across the sample and its position was measured using two vertically adjacent elements of a quadrant photodiode (Silicon Sensors QD50-6). From the amplified photo currents I_t, I_b, the vertical position of the light beam can be calculated as $\langle y \rangle = f \frac{I_t - I_b}{I_t + I_b}$. The factor f depends on the beam diameter and was measured in-situ by translating the detector using a micrometre stage.

The transmitted port of the beam splitter was used to monitor the Stokes parameter $S_3 = \frac{I_{\sigma+} - I_{\sigma-}}{I_{\sigma+} + I_{\sigma-}}$. We identi-

fied $S_3 = 0.99 \pm 0.01$ and $S_3 = -0.99 \pm 0.01$ with the circular states of polarization σ^+ and σ^- respectively. The amplified photo currents I_t, I_b, I_{σ^+} , and I_{σ^-} were digitally sampled (using a National Instruments PCI-6281) for 1 s at 50 kHz.

Since the signal is periodic with the modulation frequency f_{mod}, we can filter technical noise in a post-processing stage. To this end, the discrete Fourier transform is computed and only spectral components with frequencies equal to f_{mod} and higher harmonics thereof are passed.

For both circular states of polarization, $\sigma = +1$ and $\sigma = -1$, we calculated the mean of all corresponding beam positions $\langle y \rangle$ and the helicity-dependent beam shift $\delta^{\mathrm{R}} = \langle y \rangle (\sigma = +1) - \langle y \rangle (\sigma = -1)$. Both series of shift measurements were repeated five times. We report the mean value and standard deviation of the mean in Figure 4.

We have extensively characterized systematic errors in our system and found that the observed position of the light beam depends on the state of polarization even if no sample is present in the beam path. The magnitude of this apparent beam shift ranges from 5 to 400 nm and depends on the transverse alignment of the collimating lens and the presence of polarization optics in the beam path. To account for this effect, the shift measurements $\Delta(\theta) = \Delta^{\mathrm{R}}(\theta) - \Delta^{\mathrm{R}}(0^\circ)$ reported here are corrected with respect to the raw data points $\Delta^{\mathrm{R}}(\theta)$.

ACKNOWLEDGEMENTS

The authors thank Christian Gabriel for fruitful discussions and for his contribution in the initial stage of the experiment.

* andrea.aiello@mpl.mpg.de

[1] M. Onoda, S. Murakami, and N. Nagaosa, Physical Review Letters **93**, 083901 (2004), arXiv:cond-mat/0405129.
[2] O. Hosten and P. Kwiat, Science **319**, 787 (2008).
[3] X. Yin, Z. Ye, J. Rho, Y. Wang, and X. Zhang, Science **339**, 1405 (2013).
[4] A. Aiello, N. Lindlein, C. Marquardt, and G. Leuchs, Physical Review Letters **103**, 100401 (2009).
[5] J. Korger, A. Aiello, C. Gabriel, P. Banzer, T. Kolb, C. Marquardt, and G. Leuchs, Applied Physics B **102**, 427 (2011), arXiv:1102.1626.
[6] F. Goos and H. Hänchen, Annalen der Physik **436**, 333 (1947).
[7] F. I. Fedorov, Dokl. Akad. Nauk. SSSR **105**, 465 (1955).
[8] C. Imbert, Physical Review D **5**, 787 (1972).
[9] A. Aiello, New Journal of Physics **14**, 013058 (2012).
[10] F. Pillon, H. Gilles, and S. Fahr, Applied Optics **43**, 1863 (2004).
[11] J.-M. Ménard, A. E. Mattacchione, M. Betz, and H. M. van Driel, Optics Letters **34**, 2312 (2009).
[12] M. Merano, A. Aiello, G. W. 't Hooft, M. P. van Exter, E. R. Eliel, and J. P. Woerdman, Optics Express **15**, 15928 (2007).
[13] H. Schilling, Annalen der Physik **471**, 122 (1965).
[14] A. Dooghin, N. Kundikova, V. Liberman, and B. Zel'dovich, Physical Review A **45**, 8204 (1992).
[15] C. C. Leary, M. G. Raymer, and S. J. van Enk, Physical Review A **80**, 061804 (2009), arXiv:0905.3778.
[16] V. Liberman and B. Zel'dovich, Physical Review A **46**, 5199 (1992).
[17] K. Y. Bliokh and Y. Bliokh, Physics Letters A **333**, 181 (2004).
[18] K. Y. Bliokh and Y. Bliokh, Physical Review Letters **96**, 073903 (2006), arXiv:physics/0508093.
[19] A. Aiello and J. P. Woerdman, Optics Letters **33**, 1437 (2008), arXiv:0804.1895.
[20] K. Y. Bliokh, A. Niv, V. Kleiner, and E. Hasman, Nature Photonics **2**, 748 (2008), arXiv:0810.2136.
[21] N. B. Baranova, A. Y. Savchenko, and B. Y. Zel'dovich, Soviet Journal of Experimental and Theoretical Physics Letters **59**, 232 (1994).
[22] K. Bliokh, Y. Gorodetski, V. Kleiner, and E. Hasman, Physical Review Letters **101**, 030404 (2008).
[23] K. Y. Bliokh, A. Aiello, and M. A. Alonso, in *The angular momentum of light*, edited by D. L. Andrews and M. Babiker (Cambridge University Press, 2012).
[24] A. Bekshaev, K. Y. Bliokh, and M. Soskin, Journal of Optics **13**, 053001 (2011), arXiv:1011.0862.
[25] A. Y. Bekshaev, Journal of Optics A: Pure and Applied Optics **11**, 094003 (2009).
[26] K. Y. Bliokh and F. Nori, Physical Review Letters **108**, 5 (2012), arXiv:1112.5618.
[27] M. V. Berry, Journal of Optics A: Pure and Applied Optics **11**, 094001 (2009).
[28] J. Durnin, C. Reece, and L. Mandel, Journal of the Optical Society of America **71**, 115 (1981).
[29] B.-Y. Liu and C.-F. Li, Optics Communications **281**, 3427 (2008).
[30] Y. Fainman and J. Shamir, Applied Optics **23**, 3188 (1984).
[31] J. W. Goodman, *Introduction to Fourier optics*, 3rd ed. (Roberts & Co, Englewood, USA, 2005).
[32] H. A. Haus, American Journal of Physics **61**, 818 (1993).
[33] A. Aiello, C. Marquardt, and G. Leuchs, Optics Letters **34**, 3160 (2009).

SUPPLEMENTARY INFORMATION

A. Phenomenological polarizer model and characterization of our real-world polarizer

In this section, we describe a geometric polarizer model, analogously to the work by Fainman and Shamir,[30] and determine empirical parameters relevant for the actual polarizer used in our experiment. Here, the interaction of an arbitrarily oriented polarizer with a plane wave is discussed while we deal with real light beams in the subsequent section on beam shifts.

A polarizer is an optical device that alters the state of polarization and intensity of a plane wave without effecting its direction of propagation $\hat{\boldsymbol{\kappa}} = \boldsymbol{k}/k$. The polarizer used within this work can be described by a real-valued unit vector $\hat{\boldsymbol{P}}_a$ describing its absorbing axis. Projecting $\hat{\boldsymbol{P}}_a$ onto the transverse plane of the electric field yields to an effective absorbing axis

$$\hat{\boldsymbol{a}}(\hat{\boldsymbol{\kappa}}) = \frac{\hat{\boldsymbol{P}}_a - (\hat{\boldsymbol{P}}_a \cdot \hat{\boldsymbol{\kappa}})\,\hat{\boldsymbol{\kappa}}}{\sqrt{1 - (\hat{\boldsymbol{P}}_a \cdot \hat{\boldsymbol{\kappa}})^2}}. \tag{SI.1}$$

Thus, the electric field transmitted across an idealized polarizer is

$$\tilde{\boldsymbol{E}}_T = \tilde{\boldsymbol{E}}_I - \hat{\boldsymbol{a}}\left(\hat{\boldsymbol{a}} \cdot \tilde{\boldsymbol{E}}_I\right) = \hat{\boldsymbol{t}}\left(\hat{\boldsymbol{t}} \cdot \tilde{\boldsymbol{E}}_I\right), \tag{SI.2}$$

where $\tilde{\boldsymbol{E}}_I = \tilde{\boldsymbol{E}}_I(\boldsymbol{k})$ is the amplitude of the plane wave $\exp(i\,\hat{\boldsymbol{\kappa}} \cdot \boldsymbol{r})$, and

$$\hat{\boldsymbol{t}}(\hat{\boldsymbol{\kappa}}) = \hat{\boldsymbol{a}}(\hat{\boldsymbol{\kappa}}) \times \hat{\boldsymbol{\kappa}} = \frac{\hat{\boldsymbol{P}}_a \times \hat{\boldsymbol{\kappa}}}{|\hat{\boldsymbol{P}}_a \times \hat{\boldsymbol{\kappa}}|} \tag{SI.3}$$

is the effective transmitting axis.

However, real-world polarizers have finite extinction ratios and an experimental characterization shows that the effectiveness of our polarizer decreases when tilted (Supplementary Figure 1). Thus, we have found it convenient to phenomenologically describe the transmitted light field as

$$\tilde{\boldsymbol{E}}_T = \tau_t\,\hat{\boldsymbol{t}}\left(\hat{\boldsymbol{t}} \cdot \tilde{\boldsymbol{E}}_I\right) + \tau_a\,\hat{\boldsymbol{a}}\left(\hat{\boldsymbol{a}} \cdot \tilde{\boldsymbol{E}}_I\right). \tag{SI.4}$$

Here, we employ two empirical parameters, $\tau_a(\theta)$ and $\tau_t(\theta)$, depending on the angle θ between the propagation direction $\hat{\boldsymbol{\kappa}}$ and the unit vector perpendicular to the surface of the polarizer. We have found the following set of parameters to be in good agreement with both the observed transmission and beam shifts:

$$\tau_t(\theta) = 1 - 1.2\,\exp(-12\,\cos\theta) \tag{SI.5}$$
$$\tau_a(\theta) = 0.51\,\exp(-1.3\,\cos\theta) \tag{SI.6}$$

A more detailed study of tilted polarizers will be published elsewhere.

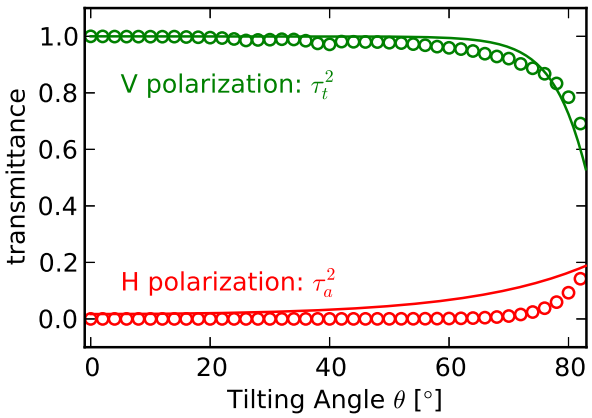

Supplementary Figure 1. **Transmittance of light beams across the polarizer as a function of the tilting angle θ and the incident state of polarization.** The polarizer is aligned such that at normal incidence ($\theta = 0°$) vertical (V) polarization is transmitted and horizontal (H) polarization is blocked. We observe how the transmittance changes when the polarizer is rotated around the vertical axes and compare the experimental data (circles) to our phenomenological model (SI.4) (solid lines).

B. Calculation of beam shifts occurring at an oblique polarizer according to our phenomenological model

In this section, we adapt the theory for the geometric spin Hall effect of light originally calculated for a different type of polarizer[5] to our phenomenological model. To this end, we express the polarizer's absorbing axis

$$\hat{\boldsymbol{P}}_a = \hat{\boldsymbol{x}}' = \cos\theta\,\hat{\boldsymbol{x}} + \sin\theta\,\hat{\boldsymbol{z}} \tag{SI.7}$$

in the global reference frame $\{\hat{\boldsymbol{x}}, \hat{\boldsymbol{y}}, \hat{\boldsymbol{z}}\}$, aligned with the direction $\hat{\boldsymbol{z}}$ of beam propagation.

The incident beam $\boldsymbol{E}_I(\boldsymbol{r})$ is circularly polarized and well-collimated, i.e. it has a low divergence θ_0, with a Gaussian transverse intensity profile. This is expanded in a plane wave basis with amplitudes $\tilde{\boldsymbol{E}}_I(\hat{\boldsymbol{\kappa}})$ such that the $\hat{\boldsymbol{\kappa}}$-dependent projection (SI.4) can be applied.

As a consequence of our polarizer model, the electric field $\boldsymbol{E}_T(\boldsymbol{r})$ after transmission across such a polarizer, is a superposition of two orthogonally polarized field components, $\boldsymbol{E}_x(\boldsymbol{r})$ and $\boldsymbol{E}_y(\boldsymbol{r})$. Thus, the electric field energy density distribution (at the detection plane $z = 0$)

$$|\boldsymbol{E}_T(x,y)|^2 = \underbrace{|\boldsymbol{E}_T \cdot \hat{\boldsymbol{x}}|^2}_{=|E_x|^2} + \underbrace{|\boldsymbol{E}_T \cdot \hat{\boldsymbol{y}}|^2}_{=|E_y|^2} + \underbrace{|\boldsymbol{E}_T \cdot \hat{\boldsymbol{z}}|^2}_{\approx 0} \tag{SI.8}$$

can be decomposed analogously.

Geometric SHEL manifests itself as a transverse displacement $\langle y \rangle$ of the transmitted light beam's barycentre. The total electric energy density $|\boldsymbol{E}_T|^2$ and both of its non-vanishing components undergo such a shift. Since this spatial displacement is independent from the

z coordinate, we restrict the discussion to the detection plane at $z = 0$. It is convenient to write the total energy density's barycentre

$$\langle y \rangle_{|\boldsymbol{E}_T|^2} = w_x \langle y \rangle_{|E_x|^2} + w_y \langle y \rangle_{|E_y|^2} \tag{SI.9}$$

as a weighted sum of the relative shifts occurring for the horizontally and vertically polarized components respectively. Here,

$$\langle y \rangle_u = \frac{\iint y\, u(x,y)\, \mathrm{d}\, x\, \mathrm{d}\, y}{\iint u(x,y)\, \mathrm{d}\, x\, \mathrm{d}\, y} \tag{SI.10}$$

denotes the centre of mass along the $\hat{\boldsymbol{y}}$ direction calculated with respect to a scalar distribution $u(x, y)$. The integration spans the whole detection plane.

The weights

$$\begin{aligned} w_x(\theta) &= \frac{\iint E_x^2(x,y)\, \mathrm{d}\, x\, \mathrm{d}\, y}{\iint |\boldsymbol{E}|^2(x,y)\, \mathrm{d}\, x\, \mathrm{d}\, y} \\ &= \frac{\tau_a^2(\theta)}{\tau_a^2(\theta) + \tau_t^2(\theta)} + \mathcal{O}(\theta_0^2) \quad \text{and} \end{aligned} \tag{SI.11}$$

$$w_y(\theta) = \frac{\tau_t^2(\theta)}{\tau_a^2(\theta) + \tau_t^2(\theta)} + \mathcal{O}(\theta_0^2) \tag{SI.12}$$

introduced in (SI.9) depend on the empirical parameters τ_t and τ_a (SI.5). Finally, we can calculate the relative shifts

$$\begin{aligned} \frac{\langle y \rangle_{|E_i|^2}}{\lambda} &= \frac{\iint\limits_{x,y} y\, |E_i|^2\, \mathrm{d}\, x\, \mathrm{d}\, y}{\iint\limits_{x,y} |E_i|^2\, \mathrm{d}\, x\, \mathrm{d}\, y} \\ &= \sigma\, \frac{\tan\theta}{2\,\pi}\, f_i(\theta) + \mathcal{O}(\theta_0^2), \end{aligned} \tag{SI.13}$$

where the factors

$$f_x(\theta) = 1 - \frac{\tau_t(\theta)}{\tau_a(\theta)} < 0 \quad \text{and} \tag{SI.14a}$$

$$f_y(\theta) = 1 - \frac{\tau_a(\theta)}{\tau_t(\theta)} > 0 \tag{SI.14b}$$

depend critically on the performance of the polarizer.

Note that, since the transmission coefficients are real and positive and $1 \geq \tau_t > \tau_a$ (Supplementary Figure 1), these relative shifts have opposite signs. Consequently, the displacement of the total energy density

$$\frac{\langle y \rangle_{|\boldsymbol{E}_T|^2}}{\lambda} = \sigma\, \frac{\tan\theta}{2\,\pi}\, \underbrace{(w_x\, f_x + w_y\, f_y)}_{<1} \tag{SI.15}$$

is smaller than the relative shift $\langle y \rangle_{|E_{y'}|^2}$ of the vertically polarized component solely. For our realistic polarizer model, both shifts are smaller than expected for the ideal case. This matches very well with our experimental observation.

For a perfect polarizer with $\tau_a = 0$ and $\tau_t = 1$, equation (SI.15) reduces to equation (1) since $w_x\, f_x = \frac{\tau_a^2}{\tau_t^2}\left(1 - \frac{\tau_t}{\tau_a}\right) \to 0$ for $\tau_a \to 0$. This is exactly the same expression that was originally found for the polarizer model by Fainman and Shamir.[5]

C. Calculation of the geometric spin Hall effect of light at a polarizing interface

In this part, we derive in a detailed manner equation (1) for a paraxial fundamental Gaussian beam incident at an angle θ upon the surface of an *absorbing polarizer* whose absorbing axis is directed along x'. The Cartesian coordinate systems attached to the polarizing interface and to the beam are still defined as in Fig. 2A in the main text. However, now the axis x' is taken parallel to the absorbing axis of the polarizer, in order to reproduce the actual experimental conditions.

Consider the fundamental solution of the scalar paraxial wave equation[31] that we indicate with $\psi(\boldsymbol{r})$:

$$\psi(\boldsymbol{r}) = \left(\frac{k}{\pi L}\right)^{1/2} \frac{i}{1 + iz/L} \exp\left(-\frac{1}{w_0^2}\frac{x^2 + y^2}{1 + iz/L}\right), \tag{SI.16}$$

where the Rayleigh range L of the beam can be expressed in terms of the beam waist w_0 as $L = kw_0^2/2$, with $\theta_0 = 2/(kw_0) \ll 1$ denoting the angular spread of the beam. In the first-order approximation with respect to θ_0, the electric vector field of the incident beam can be written as:[32]

$$\begin{aligned} \boldsymbol{\Psi}^{\mathrm{in}}(\boldsymbol{r}) &= \hat{\boldsymbol{u}}_\sigma\, \psi(\boldsymbol{r}) + \hat{\boldsymbol{z}}\frac{i}{k}\hat{\boldsymbol{u}}_\sigma \cdot \boldsymbol{\nabla}\psi(\boldsymbol{r}) \\ &= \left[\hat{\boldsymbol{u}}_\sigma - i\hat{\boldsymbol{z}}\frac{\theta_0\,(x + i\sigma y)}{\sqrt{2}\, w_0\,(1 + iz/L)}\right]\psi(\boldsymbol{r}), \end{aligned} \tag{SI.17}$$

where $\hat{\boldsymbol{u}}_\sigma = (\hat{\boldsymbol{x}} + i\sigma\hat{\boldsymbol{y}})/\sqrt{2}$ and an overall (irrelevant) multiplicative term has been omitted. In Ref.[33] it was demonstrated that the field transmitted by an arbitrarily oriented polarizer can be written as a perturbative expansion of the form

$$\begin{aligned} \boldsymbol{\Psi}^{\mathrm{out}}(\boldsymbol{r}) = \widetilde{G}_{00}\boldsymbol{\Psi}^{\mathrm{in}}(\boldsymbol{r}) \\ - \frac{i}{k}\left[\widetilde{G}_{10}\frac{\partial\boldsymbol{\Psi}^{\mathrm{in}}}{\partial x}(\boldsymbol{r}) + \widetilde{G}_{01}\frac{\partial\boldsymbol{\Psi}^{\mathrm{in}}}{\partial y}(\boldsymbol{r})\right] \\ + O(\theta_0^2), \end{aligned} \tag{SI.18}$$

where the 3×3 matrices $\widetilde{G}_{nm}$ are defined as

$$\widetilde{G}_{nm} = \frac{k^{n+m}}{n!m!}\frac{\partial^{n+m}(\hat{\boldsymbol{n}}\hat{\boldsymbol{n}})}{\partial k_x^n \partial k_y^m}\bigg|_{k_x=0,\, k_y=0}. \tag{SI.19}$$

For our absorbing polarizer, the dyadic form

$$\hat{\boldsymbol{n}}\hat{\boldsymbol{n}} = \begin{pmatrix} n_x^2 & n_x\, n_y & n_x\, n_z \\ n_y\, n_x & n_y^2 & n_y\, n_z \\ n_z\, n_x & n_z\, n_y & n_z^2 \end{pmatrix} \tag{SI.20}$$

is defined in terms of the effective-transmission unit vector $\hat{\boldsymbol{n}} = \hat{\boldsymbol{a}} \times \hat{\boldsymbol{\kappa}} = n_x\hat{\boldsymbol{x}} + n_y\hat{\boldsymbol{y}} + n_z\hat{\boldsymbol{z}}$, where

$$\hat{\boldsymbol{a}} = \frac{\hat{\boldsymbol{x}}' - \hat{\boldsymbol{\kappa}}(\hat{\boldsymbol{\kappa}} \cdot \hat{\boldsymbol{x}}')}{\sqrt{1 - |\hat{\boldsymbol{\kappa}} \cdot \hat{\boldsymbol{x}}'|^2}}, \tag{SI.21}$$

and $\hat{\boldsymbol{\kappa}} = \boldsymbol{k}/k$. A straightforward calculation furnishes

$$\widetilde{G}_{00} = \begin{pmatrix} 0 & 0 & 0 \\ 0 & 1 & 0 \\ 0 & 0 & 0 \end{pmatrix}, \tag{SI.22a}$$

$$\widetilde{G}_{01} = \begin{pmatrix} 0 & \tan\theta & 0 \\ \tan\theta & 0 & -1 \\ 0 & -1 & 0 \end{pmatrix}, \tag{SI.22b}$$

$$\widetilde{G}_{10} = \begin{pmatrix} 0 & 0 & 0 \\ 0 & 0 & 0 \\ 0 & 0 & 0 \end{pmatrix}. \tag{SI.22c}$$

Substitution of equations (SI.22) and (SI.17) into equation (SI.18) yields to the following first-order expression for the transmitted field:

$$\begin{aligned}\boldsymbol{\Psi}^{\mathrm{out}}(\boldsymbol{r}) = \frac{\psi(\boldsymbol{r})}{\sqrt{2}}\Bigg[&- \hat{\boldsymbol{x}}\,\theta_0 \frac{y}{w_0}\frac{\sigma\tan\theta}{1+iz/L} \\ &+ \hat{\boldsymbol{y}}\,i\sigma\left(1+\theta_0\frac{y}{w_0}\frac{\sigma\tan\theta}{1+iz/L}\right) \\ &+ \hat{\boldsymbol{z}}\,\theta_0\frac{y}{w_0}\frac{\sigma}{1+iz/L}\Bigg] + O(\theta_0^2).\end{aligned} \tag{SI.23}$$

The electric field energy density, the physical quantity actually measured by a standard optical detector, is proportional to $|\boldsymbol{\Psi}^{\mathrm{out}}(\boldsymbol{r})|^2$ which can be calculated from Eq. (SI.21) as:

$$|\boldsymbol{\Psi}^{\mathrm{out}}(\boldsymbol{r})|^2 = |\psi(\boldsymbol{r})|^2\left(\frac{1}{2}+\theta_0\frac{y}{w_0}\frac{\sigma\tan\theta}{1+iz/L}\right) + O(\theta_0^2). \tag{SI.24}$$

Finally, the sought shift is calculated as the first moment of the electric field energy density distribution, namely

$$\begin{aligned}\langle y\rangle &= \frac{\iint y\,|\boldsymbol{\Psi}^{\mathrm{out}}(\boldsymbol{r})|^2 \mathrm{d}x\mathrm{d}y}{\iint |\boldsymbol{\Psi}^{\mathrm{out}}(\boldsymbol{r})|^2 \mathrm{d}x\mathrm{d}y} \\ &= \frac{\sigma}{k}\tan\theta,\end{aligned} \tag{SI.25}$$

where the integration is evaluated over all the xy plane at $z = 0$. Equation (SI.25) reproduces the result given by equation (1) in the main text.